THE COMPANY OF
Biologists

RESEARCH ARTICLE

Regulation of Rac1 translocation and activation by membrane domains and their boundaries

Konstadinos Moissoglu[1,2,*,‡‡], Volker Kiessling[3,4], Chen Wan[3,4,‡], Brenton D. Hoffman[1,2,§], Andres Norambuena[1,2,¶], Lukas K. Tamm[3,4] and Martin Alexander Schwartz[1,2,5,**,‡‡]

ABSTRACT

The activation of Rac1 and related Rho GTPases involves dissociation from Rho GDP-dissociation inhibitor proteins and translocation to membranes, where they bind effectors. Previous studies have suggested that the binding of Rac1 to membranes requires, and colocalizes with, cholesterol-rich liquid-ordered (*lo*) membrane domains (lipid rafts). Here, we have developed a fluorescence resonance energy transfer (FRET) assay that robustly detects Rac1 membrane targeting in living cells. Surprisingly, FRET with acceptor constructs that were targeted to either raft or non-raft areas indicated that Rac1 was present in both regions. Functional studies showed that Rac1 localization to non-raft regions decreased GTP loading as a result of inactivation by GTPase-activating proteins. *In vitro*, Rac1 translocation to supported lipid bilayers also required *lo* domains, yet Rac1 was concentrated in the liquid-disordered (*ld*) phase. Single-molecule analysis demonstrated that translocation occurred preferentially at *lo*–*ld* boundaries. These results, therefore, suggest that Rac1 translocates to the membrane at domain boundaries, then diffuses into raft and non-raft domains, which controls interactions. These findings resolve discrepancies in our understanding of Rac biology and identify novel mechanisms by which lipid rafts modulate Rho GTPase signaling.

KEY WORDS: Rac, FRET, Lipid rafts, Supported bilayers, Domain boundaries

INTRODUCTION

Rho-family GTPases are central to embryonic development, neuronal pathfinding, wound repair, angiogenesis and immune responses through the regulation of cytoskeletal organization, adhesion dynamics, membrane trafficking, cell cycle progression,

[1]Robert M. Berne Cardiovascular Research Center, University of Virginia, Charlottesville, VA 22908, USA. [2]Department of Microbiology, University of Virginia, Charlottesville, VA 22908, USA. [3]Center for Membrane Biology, University of Virginia, Charlottesville, VA 22908, USA. [4]Department of Molecular Physiology and Biological Physics, University of Virginia, Charlottesville, VA 22908, USA. [5]Department of Biomedical Engineering, University of Virginia, Charlottesville, VA 22908, USA.
*Present address: Laboratory of Cellular and Molecular Biology, Center for Cancer Research, National Cancer Institute, National Institutes of Health, Bethesda, MD 20892, USA. ‡Present address: Department of Biochemistry and Molecular Biology, University of British Columbia, Vancouver, BC V6T 1Z3, Canada. §Present address: Department of Biomedical Engineering, Duke University, Durham, NC 27708, USA. ¶Present address: Department of Biology, University of Virginia, Charlottesville, VA 22908, USA. **Present address: Yale Cardiovascular Research Center and Departments of Medicine and Cell Biology, Yale School of Medicine, New Haven CT 06511, USA.

‡‡Authors for correspondence (konstadinos.moissoglu@nih.gov; martin.schwartz@yale.edu)

cell survival and gene transcription (Jaffe and Hall, 2005). Their dysregulation contributes to diseases including cancer, atherosclerosis, inflammation and mental retardation. Rho GTPases are controlled by two linked regulatory cycles. First, they are activated (GTP-bound) and inactivated (GDP-bound) through the actions of guanine-nucleotide exchange factors (GEFs) and GTPase-activating proteins (GAPs), respectively. Second, activation involves dissociation from a Rho-GDP dissociation inhibitor (RhoGDI) and translocation to the plasma membrane, whereas inactivation involves re-binding to a RhoGDI and the return to the cytoplasm. Membrane targeting is mediated by both the C-terminal prenyl group and adjacent poly-basic regions. (DerMardirossian and Bokoch, 2005; Dovas and Couchman, 2005).

Previous work from our laboratory and others has suggested that when Rac1 (hereafter called Rac) associates with membranes, it does so primarily with cholesterol-rich, ordered domains on the membrane, so-called lipid rafts. Rac colocalizes with lipid raft markers in cells (del Pozo et al., 2004; Michaely et al., 1999), Rac membrane binding sites co-purify with raft fractions and Rac binding to membranes both *in vitro* and *in vivo* requires cholesterol (del Pozo et al., 2004). Despite these results, there is also evidence that the unsaturated and bulky geranyl-geranyl modification of Rac is incompatible with raft domains (Melkonian et al., 1999; Roberts et al., 2008).

Here, we report that despite the requirement for ordered membrane domains in translocation, once Rac is translocated to the membrane, much of it is found in non-raft disordered domains. This partitioning was found to influence Rac function through selective inactivation in non-raft regions. Furthermore, the apparent paradox that Rac requires ordered domains for membrane binding but is not enriched in these domains was resolved by the finding that Rac preferentially translocates at the domain boundaries before subsequent unequal partitioning into both membrane regions.

RESULTS
Development of a FRET biosensor of Rac membrane targeting

We initially sought to develop a fluorescence method to assay the membrane targeting of Rac in live cells. We employed a FRET-based approach using enhanced green fluorescent protein (EGFP)–Rac as the energy donor and membrane-bound mCherry as the acceptor. mCherry was modified by the addition of the C-terminal 20-amino-acid polybasic region and CAAX box of K-Ras (Cherry-K; Fig. 1A) (van Rheenen et al., 2007). Therefore, the assay could detect Rac membrane targeting due to increased proximity and higher FRET with the membrane-bound acceptor construct. We note that localization within the membrane could also influence FRET efficiency but, because of the large distance change that is
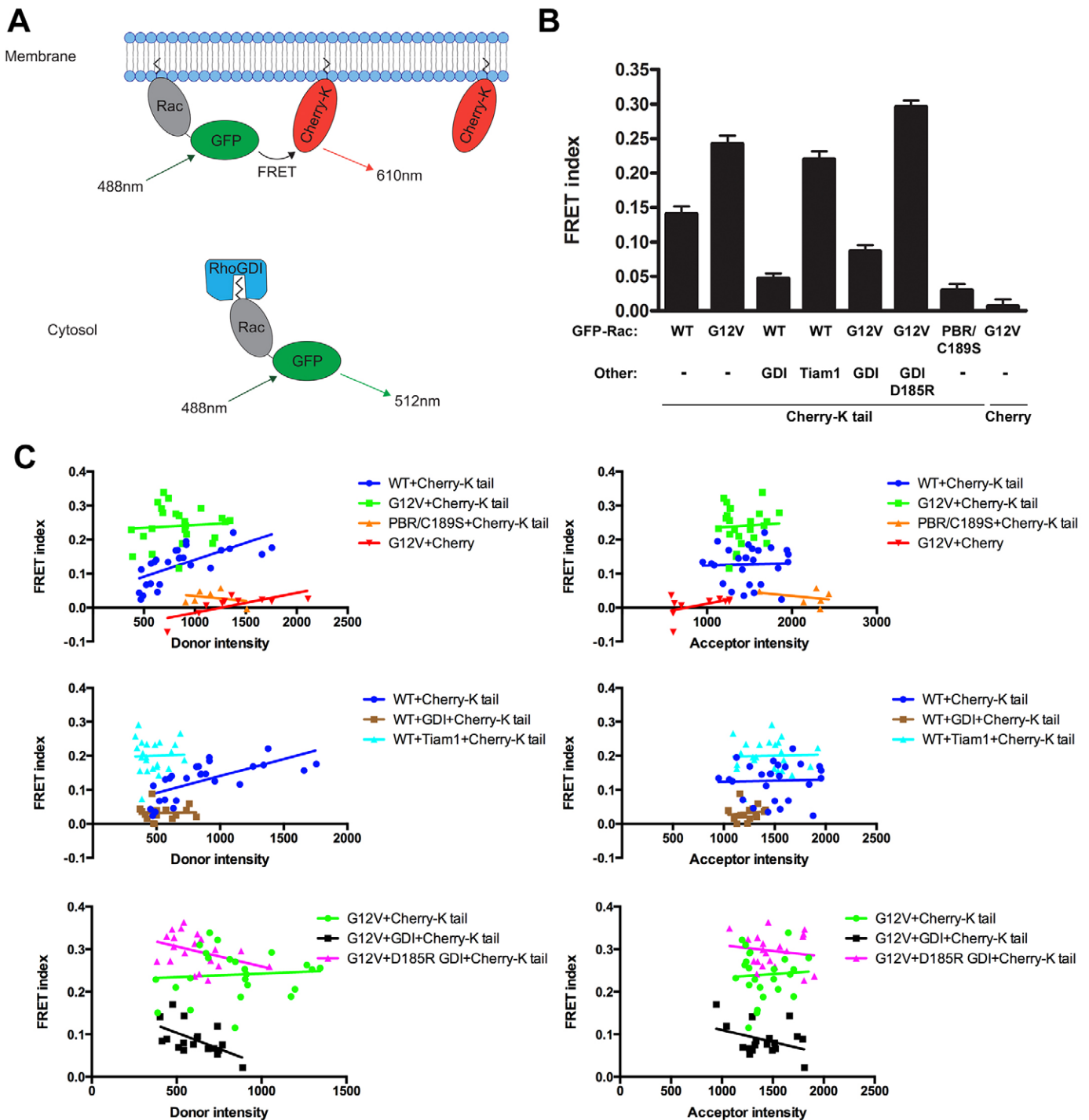
Fig. 1. FRET assay for Rac membrane targeting. (A) The method for measuring Rac membrane targeting. (B) FRET index of cells that expressed the indicated constructs. The values are means±s.e.m., n=15–26 cells in each group. P<0.001 for comparisons of wild-type (WT) Rac with G12VRac, wild-type Rac+RhoGDI or cytosolic Rac; wild-type Rac+RhoGDI with wild-type Rac+RhoGDI+Tiam1; G12VRac with G12VRac+RhoGDI or G12VRac+Cherry; G12VRac+RhoGDI to G12VRac+D185R RhoGDI (determined by one-way ANOVA). (C) Scatter plots of FRET indices relative to the donor or acceptor intensity in cells that expressed the indicated constructs. Lines represent linear regression of the corresponding data points.

associated with membrane targeting *per se*, localization within the membrane is essential. Expression of Cherry-K did not inhibit cell migration (supplementary material Fig. S1A), suggesting that it did not alter Rac function and is, thus, appropriate for use.

NIH3T3 fibroblasts were transfected with various constructs, plated on fibronectin to stimulate Rac activation and imaged live

during cell spreading (supplementary material Fig. S1B). Proper analysis of bimolecular FRET in order to yield information about the average separation distance, actual affinities or binding stoichiometry depends highly on the concentration and spatial arrangement of the probes, which are not easily determined. Thus, we choose to calculate a 'FRET index' and limit the

interpretation of our results. This metric serves as a relative measurement of interaction that can be compared to independent biochemical measurements. Because Rac localizes mainly to protrusive cell membranes, the FRET intensity at cell edges was measured (supplementary material Fig. S1C) and normalized for both acceptor and donor concentration in order to derive the FRET index. This normalization, compared with normalization to donor or acceptor intensity alone, produced values with the least dependence on donor and acceptor intensities (data not shown). The FRET index for wild-type Rac was ~five times higher than for a cytoplasmic Rac construct [a double mutant at C189S and in the polybasic region (PBR)] (Fig. 1B). It was increased further by co-expression with the Rac GEF Tiam1 or for a constitutively active Rac construct (with the mutation G12V, G12VRac) (Fig. 1B; supplementary material Fig. S1B), demonstrating that Rac activation correlates with membrane targeting, as previously observed (Abo et al., 1994; Bokoch et al., 1994).

We then performed controls for Rac targeting to the membrane. Co-expression of GFP-tagged wild-type Rac or GFP–G12VRac with the Rac inhibitor RhoGDI1 decreased FRET, whereas the inactive RhoGDI1 D185R mutant was ineffective (Fig. 1B), consistent with the ability of RhoGDI1 to inhibit Rac activation and membrane translocation (supplementary material Fig. S1D). Cytoplasmic mCherry as the acceptor yielded very low FRET, even with the G12V mutant Rac (Fig. 1B), showing that efficient FRET is dependent upon membrane localization of the acceptor. To assess whether these results depended on the expression levels of the donor and acceptor, the FRET index was plotted as a function of the donor or acceptor intensity. For the cytosolic and active Rac constructs, FRET was, essentially, independent of intensity – i.e. expression levels – over this range; however, for wild-type Rac, the FRET index increased slightly at higher expression levels (Fig. 1C). This effect might reflect saturation of the RhoGDI or RacGAP pools by Rac overexpression (Boulter et al., 2010; Stites et al., 2007). Thus, wild-type Rac was used at moderate concentrations and at consistent levels between different samples. Nonetheless, these effects are small compared with the large change in FRET upon membrane translocation and closely paralleled changes in Rac membrane targeting that have been determined previously by cell fractionation (Moissoglu et al., 2006). Overall, these results show the first robust assay for Rac1 membrane targeting in living cells.

Partitioning of Rac in membrane domains in cells

We next sought to improve the ability of the FRET sensor to detect membrane localization by taking into account Rac membrane domain partitioning (Fig. 2A). Previous studies have shown that Rac requires lipid raft domains to translocate to membranes both *in vivo* and *in vitro*, that it is present in low-density raft-enriched fractions prepared without detergent and that it localizes to raft-enriched regions in cells (del Pozo et al., 2004). However, the K-Ras construct used in the FRET assays localizes mainly to non-raft domains (Prior et al., 2001). Therefore, we reasoned that a raft-localized membrane-targeting sequence could increase FRET. Surprisingly, an mCherry acceptor construct with the H-Ras membrane targeting sequence (Cherry-H) that localizes strongly to raft domains (supplementary material Fig. S1E; Fig. S2A and Prior et al., 2001) yielded less FRET than Cherry-K (0.154 and 0.231, respectively; *P*<0.05; Fig. 2B). These FRET index values were, essentially, flat with respect to donor or acceptor intensity over the range that we examined (Fig. 2C). Qualitatively similar FRET

results were obtained when the fluorophores were switched (GFP-K or GFP-H as the FRET donor and mCherry–G12VRac as acceptor; supplementary material Fig. S2B,C); however, the apparent dynamic range was reduced.

The observed difference could, in principle, be caused by a decrease in the amount of total Rac that targets to the membrane after expression of Cherry-H or less Rac partitioning in the raft compartment where Cherry-H concentrates. Fractionation experiments showed no change in the amount of Rac in the total membrane fraction when co-expressed with Cherry-H compared with Cherry-K (supplementary material Fig. S1D). In support of the notion that the change in FRET is due to the separation of Rac from Cherry-H on the membrane, analysis of Rac distribution on sucrose density gradients showed that the vast majority of the protein was present in the heavy non-raft fractions; this distribution was also unaffected by Cherry-H or Cherry-K (supplementary material Fig. S3A–C).

To further test this hypothesis, we extracted cholesterol, by using methyl-β cyclodextrin, to disrupt membrane domains. Because methyl-β cyclodextrin can have secondary effects on Rac activation or membrane translocation (del Pozo et al., 2004), these experiments used the Rac double mutant G12V R66E (G12V/R66E Rac). This mutant is constitutively membrane-associated due to defective RhoGDI1 binding (Gandhi et al., 2004); thus, FRET changes reflect the altered partitioning in membrane domains without confounding changes in Rac membrane targeting. If membrane domain partitioning mediates the difference in FRET between mCherry-K and mCherry-H, methyl-β cyclodextrin should eliminate the difference. A concentration of methyl-β cyclodextrin was used that decreased the amount of GFP-H in the low density sucrose gradient fractions (supplementary material Fig. S2D) without substantially affecting the spreading and morphology of GFP-H- and GFP-K-expressing cells or the membrane targeting of GFP-H and GFP-K (supplementary material Fig. S2E,F). Methyl-β cyclodextrin increased FRET between Rac and GFP-H and eliminated the difference in FRET between GFP-H- and GFP-K-expressing cells (Fig. 2D and supplementary material Fig. S2G). Given that these assays probe the effects of membrane partitioning, the small changes in FRET were not unexpected. However, this issue increased concern about possible artifacts from bi-molecular FRET measurements. We, therefore, took advantage of the fact that the FRET index better reflects FRET efficiency at higher donor to acceptor ratios (donor:acceptor) (Berney and Danuser, 2003). Pixels having a donor:acceptor between 1.5 and 2.5 (among the highest values in our experiments) were specifically isolated. At high donor:acceptor, treatment with methyl-β cyclodextrin increased the FRET index for both GFP-H and GFP-K but substantially eliminated the difference between them (Fig. 2E), consistent with disruption of the lateral separation between GFP-H and GFP-K. Methyl-β cyclodextrin also decreased the difference in the distribution of GFP-H and GFP-K on sucrose gradients (Fig. 2F) but had no effect on total membrane targeting for either protein (Fig. 2G). Together, these data show that a substantial fraction of Rac1 is present in non-raft regions in cells. Although these measurements do not allow a quantifiable determination of partitioning, they suggest that Rac localizes preferentially in disordered, compared with ordered, regions.

Inactivation of Rac within non-raft membrane regions

To address the functional significance of Rac membrane domain partitioning, we examined Rac chimeras that were targeted to raft or
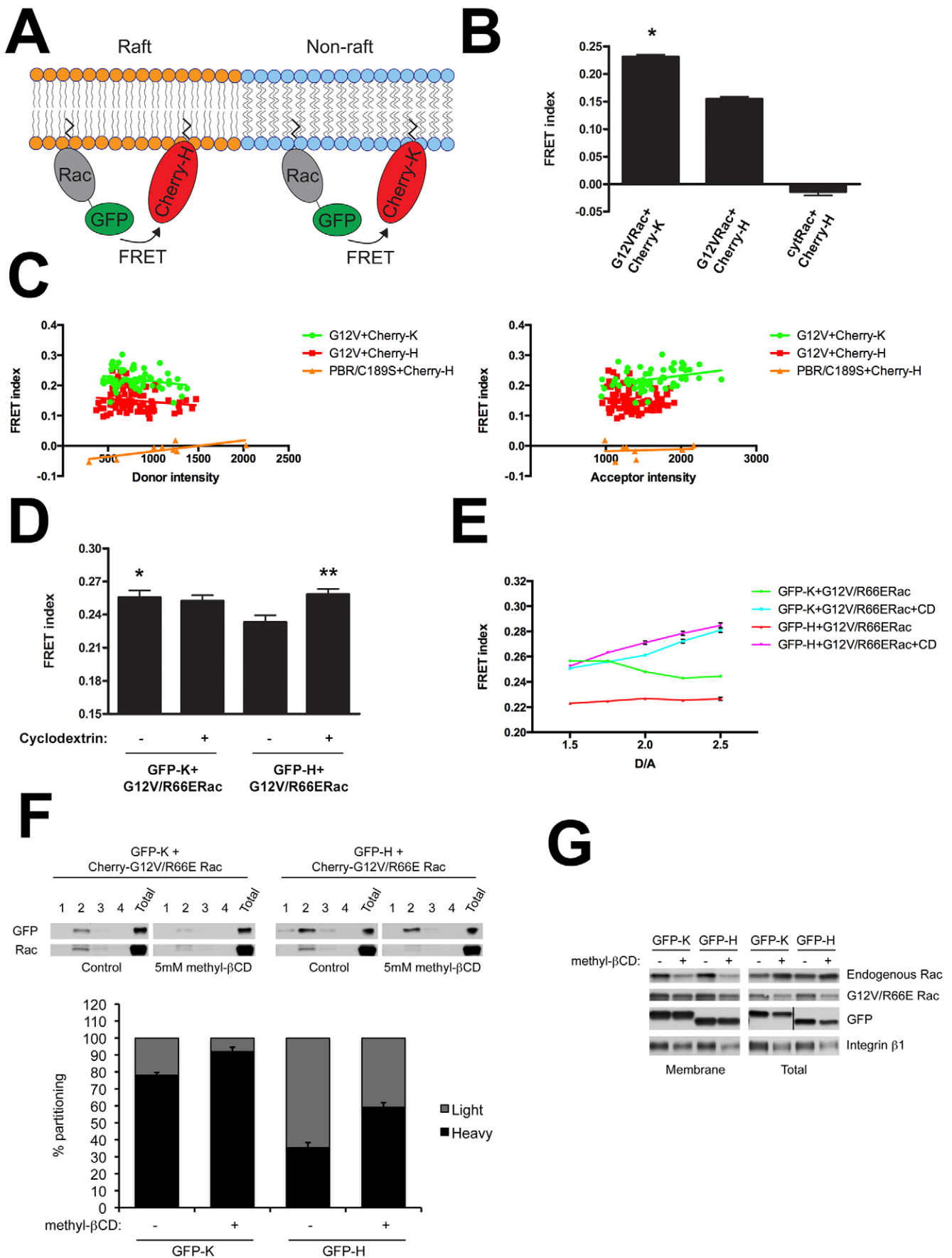
Fig. 2. See next page for legend.

Fig. 2. Rac binds strongly to non-raft membrane regions *in vivo*. (A) The method for assessing Rac partitioning in membrane domains. (B) FRET index of cells expressing GFP–G12VRac with Cherry-K ($n=63$) or Cherry-H ($n=77$), or GFP-cytosolic Rac with Cherry-H ($n=8$). The values shown are means±s.e.m., *$P<0.001$ (compared with G12VRac with Cherry-H, Student's *t*-test). (C) Scatter plots of the FRET index relative to donor or acceptor intensity in cells that expressed the indicated constructs. Lines represent linear regression of the corresponding data points. (D) FRET index of cells that expressed the indicated constructs with or without 5 mM β-methyl cyclodextrin. $n=30$–42 cells in each group. The values are means±s.e.m., *$P<0.05$, **$P<0.01$ (compared with GFP-H without cyclodextrin, one-way ANOVA). (E) Mean FRET indices (±effective s.e.m.) of selected pixels from cells expressing the indicated constructs were plotted against donor:acceptor ratios (D/A). CD, cyclodextrin. (F) Extracts from cells expressing Cherry–G12V/R66E Rac and GFP-K or GFP-H with or without 5 mM β-methyl cyclodextrin were separated on sucrose gradients. The total lysate (total) and the fractions were immunoblotted for GFP and Rac1. Representative blots of the first four light membrane fractions (lanes 1–4) are shown (upper panel). The bar graph (lower panel) depicts the percentage partitioning of GFP-K and GFP-H as the sum of the first four light fractions normalized to the total. The values shown are means± s.e.m., $n=3$. (G) Distribution of GFP-K, GFP-H and Rac in the particulate fraction (Membrane) and post-nuclear material (Total) of control or methyl-β cyclodextrin-treated cells. Results are representative of three independent experiments.

non-raft domains through H-Ras or K-Ras C-terminal sequences (termed Rac-H and Rac-K). We first analyzed the constitutively active and membrane-bound Q61L variants in order to address domain partitioning and effector binding without changes in activation state. The analysis of cell lysates on sucrose gradients confirmed that Q61LRac-H and Q61LRac-K localized, mainly, to low and high density fractions, respectively (Fig. 3A). These activated mutants also showed equivalent high levels of binding to the p21-binding domain (PBD) of PAK, indicating that altering the C-terminus did not alter effector interactions (Fig. 3B). However, the wild-type versions of these chimeras did not bind to RhoGDI1 (Fig. 3C), probably due to the altered C-terminus. Further analysis of these constructs showed that the activity of wild-type Rac-H was ~threefold higher than wild-type Rac-K in cells that had been detached and maintained in suspension or maintained in suspension and then plated onto fibronectin (Fig. 3D,E). No substantial differences were observed in cells that had been grown continuously in adherent conditions, probably owing to a low steady-state level of adhesion signaling and raft stabilization under these conditions (data not shown). To determine whether membrane domains similarly control the activity of Rac that is targeted through its own C-terminus, we analyzed the effect of methyl-β cyclodextrin on the activation state of Rac, again using the constitutively membrane-bound R66E mutant to avoid the confounding effects of membrane dissociation. Methyl-β cyclodextrin decreased binding to the PBD of PAK by ~20% (Fig. 3F). This result was confirmed by imaging a FRET probe that contained the endogenous Rac C-terminus (Raichu-Rac1–Rac1CT) (Yoshizaki et al., 2003). A positive control experiment demonstrated that the FRET index decreased after co-expression of the Rac GAP β2-chimaerin. Treatment with methyl-β cyclodextrin also reduced the FRET index at cell edges (Fig. 3G). Taken together, these studies with Rac C-terminal mutations and cyclodextrin show that localization to raft domains increases Rac activity.

To determine the mechanism by which membrane domains regulate the Rac activation state, we co-expressed Rac constructs with the Rac GEF Tiam1 or the Rac GAP β2-chimaerin. Tiam1 elevated the activity of wild-type Rac-H and wild-type Rac-K equally, suggesting that the activation by GEFs was not

domain-sensitive. By contrast, β2-chimaerin preferentially inhibited wild-type Rac-K relative to wild-type Rac-H by ~twofold (Fig. 3H,I). Notably, following cell lysis, Q61LRac-K and Q61LRac-H associated with β2-chimaerin to similar extents (Fig. 3J,K). Thus, the preferential inactivation of wild-type Rac-K is not due to a change in the intrinsic affinity for this GAP. Furthermore, β2-chimaerin primarily partitioned within heavy fractions of sucrose density gradients (Fig. 3L). Taken together, these data suggest that inactivation of Rac by GAPs occurs predominantly within non-raft regions.

Analysis of Rac localization in supported lipid bilayers

The presence and functional importance of Rac in non-raft regions was puzzling in light of published data showing that lipid rafts are required for Rac membrane translocation (del Pozo et al., 2004). To further investigate this issue, we examined Rac association with purified lipid bilayers that were supported on quartz surfaces (Crane and Tamm, 2004). In this system, the domains are large enough to be visualized by light microscopy; Rac membrane association can, therefore, be followed in real time using total internal reflection fluorescence (TIRF) microscopy (Wan et al., 2011), allowing measurement of both initial targeting and steady-state localization.

To probe Rac localization in this system, we used purified, prenylated and processed FLAG-tagged GFP–Rac1 in a 1:1 complex with recombinant RhoGDI1 (Fig. 4A). Symmetric supported bilayers of several compositions were examined. Membranes with the composition bPtdCho:bSphM:cholesterol (porcine brain phosphatidylcholine:porcine brain sphingomyelin:cholesterol) at 2:2:1 contained *lo* domains as circular regions within a continuous *ld* domain, as indicated by the *ld* marker Rhodamine-DPPE [1,2-dipalmitoyl phosphatidylethanolamine-*N*-(lissamine rhodamine B sulfonyl)] (Fig. 4B; two-phase bilayer). Rac showed strong nucleotide-dependent binding to these membranes (Fig. 4C,D; supplementary material Fig. S4) but bound poorly to control membranes comprising bPtdCho or synthetic POPC and cholesterol at a 4:1 ratio that did not form *lo* domains (Crane and Tamm, 2004). These results are, essentially, identical to those from studies using liposomes (del Pozo et al., 2004) and are consistent with the requirement of raft-like domains in order for Rac to translocate to membranes. Surprisingly, when the Rac that was bound to 2:2:1 membranes was visualized, which was not possible with the liposome-based system, its concentration in the *ld* phase was ~threefold higher than in the *lo* phase (Fig. 4C,D). These data, therefore, support the results from FRET measurements in cells but lead to the paradoxical conclusion that ordered domains are required for translocation but, once it is membrane-associated, Rac then concentrates in the disordered regions.

Preferential translocation of Rac at domain boundaries

These results could be explained if Rac translocates preferentially at the boundaries between *lo* and *ld* domains, but, once membrane-bound, prefers *ld* domains. To test this hypothesis, we altered the supported lipid bilayer assay to permit observation of single molecules of Rac. Isoprenylated FLAG–SNAP–Rac1 (Rac1 that had been labeled with Alexa Fluor 647 through the SNAP tag) was loaded with GTPγS and complexed with RhoGDI1. When incubated at very low concentrations (with unlabeled carrier protein complex) with the 2:2:1 membranes, the binding events of single Rac molecules could be observed as the appearance of spots that subsequently diffused in two dimensions.
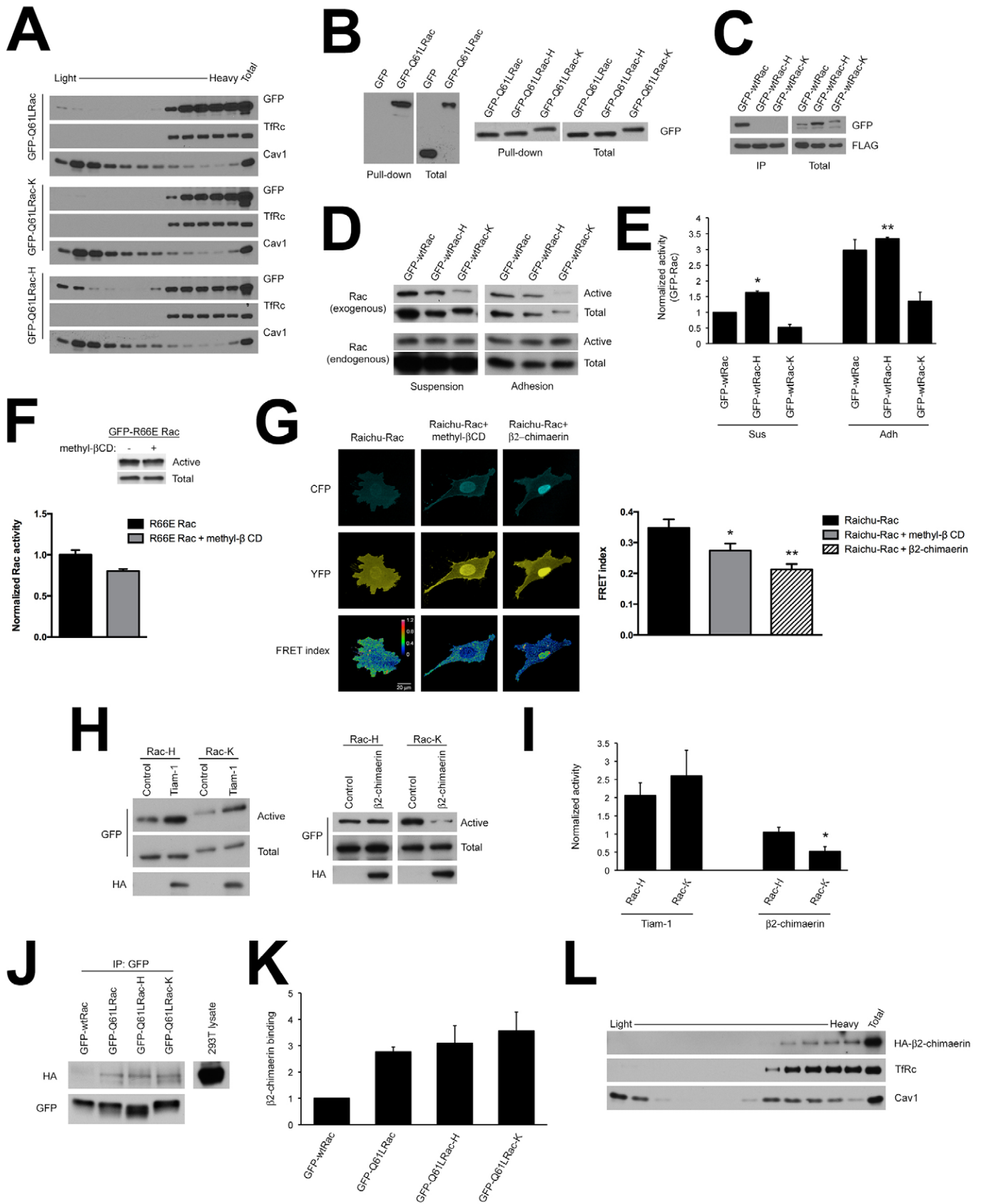
Fig. 3. See next page for legend.

Fig. 3. Increased Rac activity in proximity to rafts. (A) Rac on sucrose density gradients. Extracts, containing 0.1% TX-100, from NIH3T3 cells that expressed GFP–Q61LRac, GFP–Q61LRac-K or GFP–Q61LRac-H were separated on sucrose gradients. The fractions were immunoblotted for GFP, transferrin receptor (TfRc) and caveolin 1 (Cav1). The results are representative of three independent experiments. (B) GST–PBD pulldown assays with lysates of NIH3T3 cells that had been transfected with the indicated constructs. Representative blots from three independent experiments are shown. The pair of blots on the left show the specificity of pulldown by GFP-Q61LRac compared to GFP alone. The pair of blots on the right show equivalent binding of the indicated constructs to PBD. (C) Lysates of NIH3T3 cells expressing FLAG–RhoGDI1 and the indicated constructs were immunoprecipitated (IP) with an antibody against FLAG and analyzed by immunoblotting for GFP and FLAG. (D,E) NIH3T3 cells that stably expressed GFP–wtRac, GFP–wtRac-H or GFP–wtRac-K were harvested in suspension (Sus) or after adhesion to fibronectin (Adh) and subjected to pull down assays with the PAK-PBD, followed by Rac immunoblotting. Exogenous GFP-Rac constructs and the endogenous Rac were assessed (D). Quantification of these results (E). The fractions of active Rac (Rac that bound to the PBD) were normalized to that of GFP–wtRac in suspended cells. The values shown are means±s.e.m., $n=3$. *$P<0.01$, **$P<0.05$ (compared with the corresponding values of cells that expressed GFP–wtRac-K). (F) Lysates of NIH3T3 cells expressing GFP–R66E Rac and treated with or without 5 mM methyl-β cyclodextrin (methyl-βCD) were analyzed by pulldown assays with PAK-PBD. Samples were immunoblotted for GFP (top). Quantification of these results (bottom): the values shown are the means±s.e.m., $n=3$. *$P<0.05$ (Student's t-test). Rac activity in control cells was arbitrarily set to 1. (G) Representative images of the donor (CFP), acceptor (YFP) and FRET index from cells expressing Raichu-Rac1–Rac1CT (Raichu-Rac) under the indicated conditions (left). Bar graph (right) represents the FRET index of these cells ($n=19–23$). The values shown are means±s.e.m. *$P<0.05$, **$P<0.001$ (compared with untreated Raichu-Rac-expressing cells, Student's t-test). (H,I) NIH3T3 cells that stably expressed GFP–wtRac-H or GFP–wtRac-K were transfected with HA–Tiam1 (left panel), HA–β2-chimaerin (right panel) or empty vector. Adherent cells were analyzed by pulldown assays with PAK-PBD. Samples were immunoblotted for GFP and HA (H). These results were quantified and normalized to vector controls (I). The values shown are means±s.e.m., $n=4$. *$P<0.05$ (compared with the corresponding value of cells that expressed GFP–wtRac-H). (J,K) GFP immunoprecipitates from cells that expressed the indicated constructs were incubated with lysates of 293T cells expressing HA-tagged β2-chimaerin. The samples were immunoblotted for HA and GFP (J). Quantification of these results (K). The results were normalized to the binding by GFP–wtRac. The values shown are means±s.e.m., $n=4$. (L) The distribution of β2-chimaerin on density gradients. Membranes of NIH3T3 cells that had been transfected with HA–β2-chimaerin were isolated following non-detergent cell lysis and solubilized with 0.1% Triton X-100. Fractions (light to heavy membrane fractions) from the sucrose gradients were analyzed by immunoblotting for HA, transferrin receptor and caveolin 1. Similar results were obtained in three experiments.

The initial binding events (Fig. 4E) were identified and mapped onto epifluorescence images of the Rhodamine-DPPE-labeled bilayer (Fig. 4F). When translocation events were counted within the *ld*-phase, the *lo*-phase and a 1-μm-wide border region between the *ld*- and *lo*-phases, and then normalized to the corresponding area fraction, binding in the border region was ~three times higher than to the continuous phases (Fig. 4G). By contrast, the rates of binding to the lipid analog DiD were similar to all three regions. To validate this method, Rac binding events were analyzed as a function of the width of the boundary zone. We found that partitioning into the boundary zone was constant up to 1 μm but decreased at larger values (data not shown). Furthermore, we performed Monte Carlo simulations to calculate the expected results for random targeting. From 100 to 5000 targeting events were randomly placed onto experimental images. The largest deviations from a uniform distribution, expected for random targeting, were 3% (data not shown). Thus, translocation

of Rac to membranes occurs preferentially at lipid phase boundaries.

DISCUSSION

This study reports the development of a FRET biosensor that monitors Rac membrane targeting in live cells. Results from experiments that used different acceptor constructs that preferentially localized at distinct membrane regions, unexpectedly, revealed substantial amounts of Rac in non-raft regions of the plasma membrane. These findings were supported by the binding of Rac to supported lipid bilayers *in vitro* and by biochemical analysis of membrane fractions. Investigations into the functional significance of this partitioning showed that membrane domain localization controls Rac activation. We further found that partitioning in non-raft regions of the membrane confers higher susceptibility to the RacGAP β2-chimaerin, which concentrates in these fractions. Whether this is a general property of Rac-specific GAPs remains to be investigated.

The presence of Rac in disordered domains was surprising in light of published data that reports that ordered domains are strictly required for Rac membrane translocation (del Pozo et al., 2004). When Rac membrane binding was studied *in vitro* using purified proteins and supported bilayers, membrane binding, again, required the presence of *lo* domains, even though Rac concentrated at a 3:1 ratio into the *ld* phase. This paradox was resolved by the finding that translocation occurs, mainly, at membrane domain boundaries. These observations resolve a contradiction in the behavior of Rac – the requirement for ordered domains in Rac translocation (del Pozo et al., 2004) would appear to conflict with the preference of geranyl-geranyl groups for disordered domains (Melkonian et al., 1999; Roberts et al., 2008). The concept that translocation occurs predominantly at *lo–ld* phase boundaries, followed by diffusion into the disordered domains, reconciles all of these results.

Recently, palmitoylation of Rac, although at low stoichiometry, was shown to contribute to the association of Rac with lipid rafts (Navarro-Lérida et al., 2012). However, the modest amount of Rac in the raft fraction in our system does not appear to be dependent on palmitoylation, as inhibition of palmitoylation by 2′-bromopalmitate did not affect either the distribution of Rac on sucrose density gradients or its solubility in Triton detergent (supplementary material Fig. S3D–G). Additionally, the thioester linkage that mediates palmitoylation would not be expected to survive the isolation procedure used for the *in vitro* experiments (Schmidt et al., 1988). Presumably, our conclusions pertain to membrane targeting of unpalmitoylated Rac. However, the higher activation of raft-localized Rac probably contributes to the high biological activity of the small palmitoylated fraction (Navarro-Lérida et al., 2012).

Taken together, these results reveal an unexpected mechanism for spatial regulation in the plane of the membrane, which is likely to be important in cell migration and other functions where local activation and de-activation of Rac is crucial. Overall, these results define a novel mechanism by which lipid rafts modulate signaling in cell membranes. The work also raises new questions. A more complete understanding of Rac dynamics will require elucidation of its movement between heterogeneous membrane domains, of the localization and activation of different GEFs and GAPs in raft, non-raft and interfacial regions of the membrane, and analysis of different types of raft domains. Answering these questions will require the development of new tools to assess and manipulate structural and functional membrane heterogeneity. Understanding how plasma membrane domain architecture
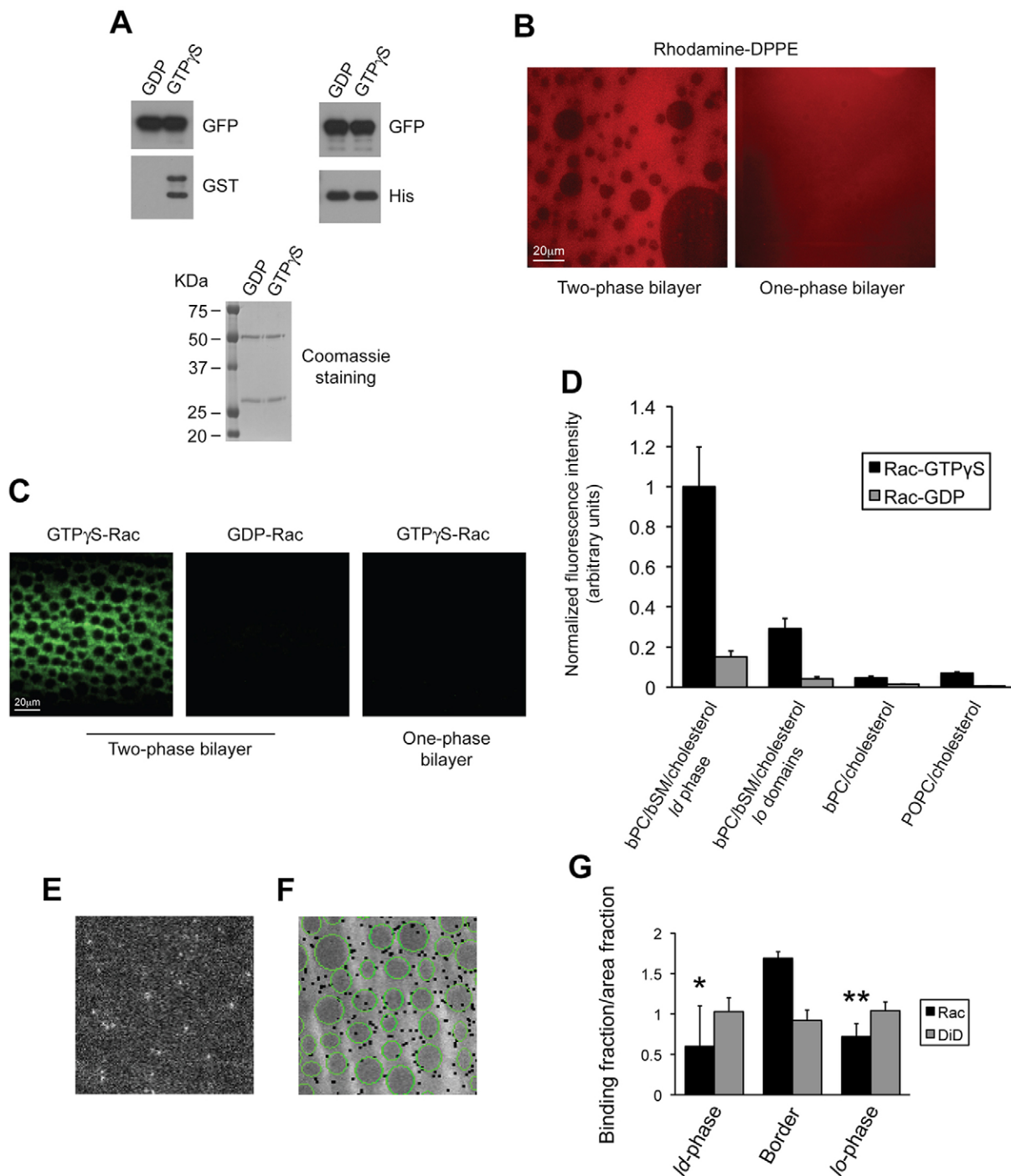
Fig. 4. Preferential translocation of Rac at domain boundaries. (A) Isoprenylated GFP–Rac for *in vitro* binding assays. Immunoprecipitated FLAG–GFP–Rac, loaded with GDP or GTPγS, was tested for nucleotide loading by adding GST–PBD, followed by elution from the beads with Flag peptide and immunoblotting for GFP and GST (upper left panel). The remaining material was incubated with excess recombinant His–RhoGDI1 in the absence of detergent before elution with Flag peptide. Complex formation was verified by immunoblotting the eluates for GFP and the His tag (upper right panel). Coomassie staining (lower panel) revealed two major species running at the expected molecular masses (50 and 28 kDa) at nearly 1:1 stoichiometry. (B) Representative images of the *ld* marker Rhodamine–DPPE in the outer leaflet of a two-phase (bPtdCho:bSphM:cholesterol, 2:2:1) or one-phase (bPtdCho:cholesterol, 4:1) bilayer. (C) Representative images of GFP–Rac (green) loaded with GTPγS or GDP and bound to a two-phase or a one-phase bilayer. (D) Normalized fluorescence intensities of GFP-Rac (loaded with GTPγS or GDP) in the *lo* and *ld* phases of the indicated two-phase bilayers after binding reaching steady state. Binding to the uniform *ld* phase of control bilayers was also recorded. The values shown are means±s.d. The mean intensity of GTPγS-loaded Rac in the *ld* phase was arbitrarily set to 1. (E) Image of single Rac molecules detected within a two-phase bilayer. Total length of the image is 31.25 μm. (F) The same bilayer as in E, labeled with Rhodamine–DPPE to identify domains. Dark *lo* domains are surrounded by a brighter, continuous *ld* phase. Overlaid green lines approximate the borders of the dark *lo* phases. Black dots represent sites of the initial appearance of single Rac molecules, accumulated over 6 min. The total length of the image is 31.25 μm. (G) Quantification of Rac or DiD binding events within the three sub-phases. The results are presented as a fraction of all detected particles (typically between 500 and 2000) normalized by the area fraction of the sub-phase. The values shown are the means±s.d., $n=5$. A value of 1 describes non-preferential binding. *$P<0.02$, **$P<0.001$ (compared with Rac in the borders, Students *t*-test).

controls local GTPase function might be relevant to the wide range of normal and pathological cell behaviors where these molecules are key regulators.

MATERIALS AND METHODS
DNA plasmids and constructs
Plasmids encoding EGFP-tagged wild-type Rac1 and G12VRac1 have been described previously (Del Pozo et al., 2002). The EGFP-tagged PBR C189S Rac1 double mutant (cytosolic Rac1), R66E Rac1 and the G12V/R66E Rac1 constructs were obtained from Amy L. Wilson-Delfosse (Case Western Reserve University, Cleveland, OH). pcDNA3-HA-C1199Tiam1 (encoding the C-terminal 1199 amino acids of Tiam1 with a hemagglutinin tag) was obtained from John G. Collard (The Netherlands Cancer Institute, Amsterdam, The Netherlands). pEGFP-Q61LRac1 was a gift from Channing J. Der (University of North Carolina, Chapel Hill, NC). pINDUCER20 was a gift from Stephen J. Elledge (Harvard Medical School, Boston, MA). pEGFP-H-Ras wild-type was obtained from John F. Hancock (The University of Texas Health Science Center, Houston, TX). A plasmid encoding HA–β2-chimaerin was from Marcelo G. Kazanietz (University of Pennsylvania, Philadelphia, PA). Raichu-Rac1–Rac1CT (Raichu-1034×) was obtained from Michiyuki Matsuda (Kyoto University, Kyoto, Japan). To generate FLAG–RhoGDI1, the coding sequence of human RhoGDI1 was amplified by PCR and subcloned into pFLAG-CMV4 (Sigma) using *Hind*III and *Xho*I sites. The D185R point mutation on RhoGDI1 was introduced using standard mutagenesis procedures.

pcDNA3-Cherry-K (also named Cherry-CAAX), carrying the C-terminal targeting sequence of K-Ras was a gift from John S. Condeelis (Albert Einstein College of Medicine, NY). To generate pcDNA3-Cherry-H, the sequence of K-Ras was excised using *Eco*RI and *Not*I, and replaced by a DNA oligo duplex that encoded the C-terminal ten amino acids of H-Ras and comprised overhangs of the same restriction sites. Similarly, DNA oligo duplexes encoding the same targeting sequences of K-Ras and H-Ras, and carrying *Eco*RI and *Bam*HI overhangs, were subloned into pEGFP-C1 (Clontech).

FLAG–Cherry–G12VRac1, FLAG–Cherry–G12V/R66E Rac1 and FLAG–EGFP–wtRac1 were generated by ligating PCR products encoding the various Rac sequences with FLAG-Cherry or FLAG-EGFP into pcDNA3.1(+). The Rac fragment was flanked by *Bsp*EI and *Eco*RI sites. FLAG-Cherry and FLAG-EGFP fragments were produced by PCR using the Cherry and EGFP sequences as templates and adding the FLAG-tag nucleotide sequence at the 5′-end of the forward primer. PCR products were flanked by *Nhe*I and *Bsp*EI restriction sites.

pcDNA3.1(+)-FLAG-SNAP-wtRac1 was generated in two steps. First, a PCR fragment encoding wild-type Rac was subcloned into pSNAP-tag(m) (New England Biolabs) using *Bam*HI and *Xho*I. The resulting SNAP-Rac1 sequence was used as template for PCR using a forward primer that contained the FLAG-tag nucleotide sequence at its 5′-end. The final product was flanked by *Eco*RI and *Xho*I sites and subcloned into pcDNA3.1(+).

To generate EGFP-tagged Rac-H and Rac-K, pEGFP-Q61LRac and pEGFP-wtRac were used as templates for PCR to amplify the corresponding Rac sequences, lacking the last 12 nucleotides. PCR products were flanked by *Xho*I and *Apa*I (for Q61LRac) and *Bsp*EI and *Apa*I (for wild-type Rac) restriction sites. DNA duplexes encoding the H-Ras and K-Ras targeting sequences (described above) comprised *Apa*I and *Eco*RI restriction site overhangs. After excision of full-length Q61LRac (using *Xho*I and *Eco*RI) and wild-type Rac (using *Bsp*EI and *Eco*RI), PCR products and DNA duplexes were ligated in-frame with EGFP.

EGFP-wtRac-H and EGFP-wtRac-K were recombined into pINDUCER20 as described previously (Meerbrey et al., 2011).

Antibodies
Antibodies used in this study include: monoclonal (B-2) or polyclonal (FL) against GFP (Santa Cruz Biotechnology), monoclonal against Rac (clone 23A8, Upstate Biotechnology), monoclonal against FLAG (clone M2, Sigma-Aldrich), monoclonal against transferrin receptor (clone H68.4, Invitrogen), polyclonal against caveolin 1 (N-20, Santa Cruz

Biotechnology), monoclonal against GST (clone B-14, Santa Cruz Biotechnology), polyclonal against His (H-15, Santa Cruz Biotechnology), peroxidase-conjugated monoclonal antibody against HA (clone BMG-3F10, Sigma) and horseradish-peroxidase-conjugated secondary antibodies against mouse and rabbit IgGs (Jackson ImmunoResearch). SDS-PAGE, western blotting and Coomassie staining were performed using standard procedures.

Cell culture and live-cell microscopy
NIH3T3 cells were grown in Dulbecco's modified Eagle's medium (DMEM) supplemented with penicillin, streptomycin (Invitrogen) and 10% calf serum (Atlanta Biologicals). DNA plasmids were transfected with Effectene according to the manufacturer's instructions (Qiagen), and cells were analyzed 24 h after transfection. For adhesion experiments, cells were serum-starved (0%) for 3 h, detached with enzyme-free cell dissociation solution (Millipore), held in suspension with 0.5% methylcellulose for 90 min and re-plated for 30 min in serum-free media onto dishes that had been coated with 2 µg/ml fibronectin.

For live-cell microscopy, cells were seeded for 2–3 h at low density on No. 1.5 microscope cover glass (Corning) that had been coated with fibronectin at 2 µg/ml in Phenol-Red-free DMEM (Invitrogen). Where indicated, methyl-β-cyclodextrin (5 mM) was added to the medium for 45 min, the cells were then washed and incubated in regular medium for 30 min. Images for FRET were obtained using a Zeiss LSM510 confocal microscope with a Plan-Neofluor 40× NA=1.3 DIC oil objective and a heated stage at 37℃ (University of Virginia Advanced Microscopy Facility). EGFP and mCherry were excited with 488-nm Argon and 543-nm HeNe laser lines, respectively. A NFT 545 beam splitter and the following filters were used: EGFP, band-pass 505–530; mCherry and FRET, long-pass 560. Images for Raichu-Rac1–Rac1CT FRET were obtained by using a Plan-Apochromat 63× NA=1.4 DIC oil objective. Cyan fluorescent protein (CFP) and yellow fluorescent protein (YFP) were excited with 458-nm and 514-nm Argon laser lines, respectively. A NFT 505 beam splitter and the following emission filters were used: band-pass 470–510 for CFP; long-pass 530 for YFP and FRET.

Segmentation of cell edges
All calculations were performed in IDL (Exelis). Because histograms of the acceptor intensity consisted of two peaked distributions, the background threshold was either set to the intensity at the minimum in the histogram between these distributions or manually selected. A binary mask was created, representing the image portions above the background threshold and subjected to a morphological close operation to create solid objects. The largest object was selected for further analysis. A contour drawing algorithm was then used to determine the cell boundary. A binary image representing the entire cell was subjected to a morphological erode function with a characteristic distance of 40 pixels and used to determine an interior boundary. The area between these two boundaries was used to determine the cell edge (typical width of 4–6 µm). Pixels from this area in all image channels were used for further analysis.

FRET analysis
FRET analysis was performed as described previously (Grashoff et al., 2010) with small alterations that were appropriate for a bi-molecular FRET biosensor. Image analysis was performed by using custom-written programs in IDL (ITT Visual Information Systems). FRET corrections were performed with non-linear spectral bleed-through corrections using the following equation:

$$cFRET = FRET - dbt(I_D)I_D - abt(I_A)I_A.$$

Here cFRET is the corrected FRET image, I_D is the intensity of the donor image, I_A is the intensity of the acceptor image, dbt is donor bleed-through, and abt is acceptor bleed-through. Other potential corrections were calculated and found to be negligible. FRET index was then calculated as:

$$\text{FRET Index} = \frac{\text{cFRET}}{I_A I_D} \times 1000.$$

This index was chosen as it showed the least dependence on donor or acceptor concentration. FRET index images were selected based on the intensity of the corresponding donor and acceptor images being within a specified range – in the middle of observed expression levels. Thus, the data had a good signal-to-noise ratio and were, probably, not subject to large overexpression artifacts.

For partitioning experiments where FRET changes were small, we used data with a donor:acceptor ratio that was within a certain range – between 1.5 and 2.5. It should be noted that donor:acceptor is an intensity and not the molar ratio of donor to acceptor. The above range was chosen because previous work has shown that the FRET index is more likely to correlate with FRET efficiency at high donor:acceptor values (Berney and Danuser, 2003). The donor:acceptor for every pixel in multiple images was calculated. Data were binned and averaged.

For experiments with the Raichu-Rac1–Rac1CT probe, the FRET index was calculated as:

$$\text{FRET Index} = \frac{\text{cFRET}}{I_A}.$$

Preparation of Rac–RhoGDI complexes
293T cells that expressed FLAG–EGFP–wtRac or FLAG–SNAP–wtRac were scraped and homogenized in a buffer containing 10 mM Tris-HCl pH 7.5, 1 mM dithiothreitol (DTT), 0.25 M sucrose and a cocktail of protease inhibitors (Sigma). Nuclei and unbroken cells were removed by centrifugation at 1000 g for 10 min at 4℃, and the post-nuclear supernatant was centrifuged at 150,000 g for 20 min at 4℃ to separate the cytosolic and particulate fractions. The particulate fraction was then dissolved in the same buffer containing 1% β-octylglucoside. The lysates were incubated with M2-antibody–agarose beads (Sigma), the beads were then washed. For nucleotide loading, the beads were treated with 2 mM EDTA followed by the addition of 20 µM GDP or GTPγS in the presence of 10 mM MgCl$_2$. Loading was verified by binding to GST–PBD (p21 binding domain of PAK1, 10 µg). Immune complexes were then washed using buffer without detergent and incubated with 40 µg of bacterially expressed His-tagged RhoGDI1 for 2 h at 4℃. Concurrently with RhoGDI binding, FLAG–SNAP–wtRac was labeled with SNAP-Surface Alexa Fluor 647 (New England Biolabs) according to the manufacturer's instructions. Complexes were then eluted with 3×FLAG peptide (Sigma) and analyzed by western blotting or Coomassie staining using standard procedures.

Large unilamellar vesicles
The desired lipids were co-dissolved in chloroform or chloroform in methanol. After drying for 1 h in a vacuum, the resulting residue was suspended in HKE buffer (25 mM HEPES, 100 mM KCl, 1 mM EGTA, pH 7.4), rapidly vortexed, freeze-thawed five times by alternate submersion in liquid N$_2$ and a water bath at 40℃, and then extruded by 15 passes through two polycarbonate membranes with a pore diameter of 100 nm (Avestin, Ottawa, ON). Vesicles were stored at 4℃ for not more than 5 days before use.

Quartz slides
Slides (40×25×1 mm^3) were purchased from Quartz Scientific (Fairport Harbor, OH). They were cleaned by boiling in Contrad detergent for 10 min and then sonicating, while still in detergent, for 30 min, followed by extensive rinsing with water, methanol and water again. Remaining organic residues were removed by immersion in three volumes of sulfuric acid to one volume of 30% hydrogen peroxide, followed by extensive rinsing in water. Immediately before use, slides were further cleaned for 10 min in an argon plasma sterilizer (Harrick Scientific, Ossining, NY).

Tethered polymer-supported bilayers
Bilayers were formed by a combined Langmuir-Blodgett/Vesicle Fusion (LB/VF) technique. bPtdCho, bSphM and Rhodamine-DPPE were purchased from Avanti Polar Lipids (Alabaster, AL); cholesterol was purchased from Sigma. A lipid monolayer containing 3% DPS (custom synthesized polymer-lipid molecule consisting of dimyristoylphosphatidylethanolamine, polyethyleneglycol and a triethoxysilane group; Shearwater Polymers, Huntsville, AL) was spread from a chloroform solution onto a pure water surface in a Nima 611 Langmuir-Blodgett trough (Nima, Conventry, UK). The solvent was allowed to evaporate for 10 min, and the monolayer was compressed at a rate of 10 cm^2/min to reach a surface pressure of 32 mN/m and equilibrated for 5–10 min. A clean quartz slide was then rapidly (200 mm/min) dipped into the trough and slowly (5 mm/min) withdrawn, while a feedback circuit maintained a constant surface pressure and monitored the transfer of lipids onto the substrate by measuring the change in surface area. The resulting monolayer on the solid support is known as the Langmuir-Blodgett monolayer. The DPS molecules were tethered to the surface by drying the coated slides in a desiccator at room temperature overnight and subsequently curing them in a 70℃ oven for 40 min. The slides were then transferred to a desiccator, allowed to equilibrate at room temperature and, typically, used on the same day.

Slides with tethered polymer-supported Langmuir-Blodgett monolayers were placed in a custom built flow-through chamber. A 0.1 mM suspension of large unilamellar vesicles in HKE buffer was slowly injected into the chamber and incubated at room temperature for 35 min. The excess vesicles were washed out by rinsing with HKE buffer.

Binding of Rac to supported bilayers
Solutions of FLAG–GFP–Rac (250 ng/ml) or Alexa-647-labeled FLAG-SNAP-Rac (25 ng/ml) in TIRF buffer (25 mM HEPES, 100 mM KCl, 1 mM EDTA, 1 mM ascorbic acid, 1 mM DTT, pH 7.4) were incubated with 10 mM bPtdCho–cholesterol (4:1) vesicles for 15 min at room temperature followed by centrifugation at 13,000 r.p.m. on a benchtop centrifuge (Eppendorf 5415R, Eppendorf, Germany) for 5 min to remove non-specific hydrophobic species. Supernatants were then injected into the flow-through chamber containing a supported bilayer. The lipid analog DiD (1,1′-Dioctadecyl-3,3,3′,3′-tetramethylindodicarbocyanine perchlorate; Molecular Probes) was used at 1 µg/ml in TIRF buffer. The binding process was monitored for ~1 h by TIRFM, and images were recorded and stored every 30 s (GFP–Rac) or every 1 s (Alexa-Fluor-647–SNAP–Rac and DiD). For single molecule experiments, epifluorescence images of the Rhodamine-DPPE-labeled monolayer of the same bilayer area were acquired before and after Rac binding.

Fluorescence microscopy of supported bilayers and image analysis
Images were recorded on a Zeiss Axiovert 200 fluorescence microscope (Carl Zeiss, Thornwood, NY) equipped with a 63× water immersion objective (Zeiss; NA=0.95) and an electron multiplying charge-coupled device (EMCCD) cooled to −70℃ (iXon DV887ESC-BV; Andor, Belfast, UK) as a detector. Images were acquired by using in-house software written in LabVIEW (National Instruments, Austin, TX). For epifluorescence, a mercury lamp was used as a light source. Bilayers that had been stained with Rhodamine–DPPE were illuminated through a 540-nm band-pass filter (D540/25, Chroma, Brattleboro, VT) and via a dichroic mirror (565dclp, Chroma) through the objective. Fluorescence was observed through a 605-nm band-pass filter (D605/55, Chroma). FLAG–GFP–Rac or single molecules of Alexa-Fluor-647-labeled FLAG–SNAP–Rac were imaged by using TIRFM. Light from the 514-nm line of an argon ion laser (Innova300C) or the 640-nm line of a diode laser (Cube 640; Coherent, Palo Alto, CA) was directed through a trapezoidal prism onto the quartz–buffer interface where the supported bilayer was attached. The prism–quartz interface was lubricated with glycerol to allow easy translocation of the sample chamber on the microscope stage. The laser beam was totally internally reflected at an angle of 72° from the surface normal, producing an evanescent wave that decays exponentially in the solution with a characteristic penetration depth of ~125 nm in our setup.

Images were analyzed using in-house programs written in LabVIEW (National Instruments). For GFP–Rac binding experiments, the mean intensities from *lo* and *ld* regions were extracted separately, and the binding curves of those regions were reconstructed. Typically, 10–20 measurements of intensities of *lo* and adjacent *ld* regions were taken within each image after binding had reached saturation.

For Alexa-Fluor-647–SNAP–Rac binding experiments, a single-particle tracking algorithm was used (Kiessling et al., 2006). Particles that were detected at least three times in consecutive images within a circle with a diameter of 8 pixels were recognized as membrane-bound Rac and their x/y coordinates were stored. The single molecule nature of the particles was confirmed by a single-step bleaching observation. Epifluorescence images of the Rhodamine-labeled monolayers were used to assign areas of *lo* and *ld* phases. The borders of the dark *lo* phases were approximated by assigning round or elliptic regions of interest. From these assignments, image areas were divided into three sub-phases: *lo*-phase, *ld*-phase and a 1-μm-wide (4 pixel) border region. Binding to the different sub-phases was quantified by comparing the coordinates of the detected Rac molecules with the assignment from the epifluorescence image.

Subcellular fractionation
Cells were washed with ice-cold PBS, scraped and homogenized in buffer containing 10 mM Tris-HCl (pH 7.5), 5 mM $MgCl_2$, 1 mM DTT, 0.2 M sucrose and protease inhibitor cocktail (Sigma-Aldrich). Nuclei and unbroken cells were removed by centrifugation at 1000 *g* for 10 min at 4℃, and the post-nuclear supernatant was centrifuged at 100,000 *g* for 1 h at 4℃ to separate the cytosolic and particulate fractions.

Detergent-resistant membranes
Detergent-resistant membranes were obtained by sucrose flotation after whole-cell extraction, or after solubilization of particulate fractions. Briefly, cells were lysed in ice-cold TNE buffer (25 mM Tris, pH 7.5, 150 mM NaCl, 2 mM EGTA) containing 0.05% or 0.1% Triton X-100 (v/v). Alternatively, cells were lysed without detergent and the particulate fraction was solubilized with TNE buffer containing 0.1% Triton X-100. The homogenate (1 ml) was then adjusted to 40% sucrose by the addition of 1 ml of 80% sucrose prepared in TNE that was placed at the bottom of an ultracentrifuge tube. A 5–30% discontinuous sucrose gradient was formed (0.5 ml of 5% sucrose and 2.5 ml of 30% sucrose, both in TNE) and centrifuged at 180,000 *g* for 16 h. Twelve fractions of 410 μl each were collected from the top of the centrifuge tube. Alternatively, crude Triton–resistant pellets were collected by centrifugation at 17,000 *g* for 10 min. Samples were resolved by SDS–PAGE and analyzed by immunoblotting. Immunoblots were quantified by densitometry using ImageJ software.

Stable transfectants
Lentivirus transducing EGFP–wtRac-H or EGFP–wtRac-K was produced as described previously (Meerbrey et al., 2011). NIH3T3 cells were infected (MOI: 5) for 72 h and then selected with 800 μg/ml Geneticin. For induction of protein expression, cells were treated with 250 ng/ml doxycycline for 24 h.

Active Rac pull-down assays
Assays were performed as described previously (Moissoglu et al., 2009).

Chimaerin pull down
Cells expressing GFP–wtRac, GFP–Q61LRac, GFP–Q61LRac-H or GFP–Q61LRac-K were lysed with the same buffer used for active Rac pulldown assays (see above), and lysates were subjected to GFP immunoprecipitation. Binding of β2-chimaerin was then assayed using a GAP analysis protocol described previously (García -Mata et al., 2006). Briefly, 293T cells expressing HA-tagged β2-chimaerin were lysed in 20 mM HEPES pH 7.5, 150 mM NaCl, 5 mM $MgCl_2$, 1% Triton X-100, 1 mM DTT and protease inhibitors, and the extract was incubated with the immobilized GFP–Rac proteins for 2 h at 4℃. Bound β2-chimaerin was analyzed by SDS-PAGE and immunoblotting.

Migration assays
1×10^5 cells were plated onto custom-made glass-bottomed 35-mm dishes that had been coated with 2 μg/mL fibronectin. Three hours after plating, the dishes were transferred to a custom-made heated stage that was mounted on a Nikon Diaphot-TMD inverted microscope (Nikon). The cells were imaged every 5 min for 4 h using a CoolSnap HQ Monochrome camera (Photometrics, Roper Scientific). Temperature in the medium was maintained at 37℃ and the pH was controlled by the addition of 25 mM HEPES buffer. The medium was overlaid with mineral oil to prevent evaporation. Image acquisition was controlled by ISee software (Inovision). The tracks of individual cells were analyzed using ImageJ software.

Statistics
Statistical significance was determined by using Student's *t*-test, one-way or two-way analysis of variance (ANOVA), as appropriate. Post-hoc testing was done with the Tukey-b test.

Supplementary material
Supplementary material available online at
http://jcs.biologists.org/lookup/suppl/doi:10.1242/jcs.149088/-/DC1

References
Abo, A., Webb, M. R., Grogan, A. and Segal, A. W. (1994). Activation of NADPH oxidase involves the dissociation of p21rac from its inhibitory GDP/GTP exchange protein (rhoGDI) followed by its translocation to the plasma membrane. *Biochem. J.* **298**, 585-591.
Berney, C. and Danuser, G. (2003). FRET or no FRET: a quantitative comparison. *Biophys. J.* **84**, 3992-4010.
Bokoch, G. M., Bohl, B. P. and Chuang, T. H. (1994). Guanine nucleotide exchange regulates membrane translocation of Rac/Rho GTP-binding proteins. *J. Biol. Chem.* **269**, 31674-31679.
Boulter, E., Garcia-Mata, R., Guilluy, C., Dubash, A., Rossi, G., Brennwald, P. J. and Burridge, K. (2010). Regulation of Rho GTPase crosstalk, degradation and activity by RhoGDI1. *Nat. Cell Biol.* **12**, 477-483.
Crane, J. M. and Tamm, L. K. (2004). Role of cholesterol in the formation and nature of lipid rafts in planar and spherical model membranes. *Biophys. J.* **86**, 2965-2979.
Del Pozo, M. A., Kiosses, W. B., Alderson, N. B., Meller, N., Hahn, K. M. and Schwartz, M. A. (2002). Integrins regulate GTP-Rac localized effector interactions through dissociation of Rho-GDI. *Nat. Cell Biol.* **4**, 232-239.
del Pozo, M. A., Alderson, N. B., Kiosses, W. B., Chiang, H. H., Anderson, R. G. and Schwartz, M. A. (2004). Integrins regulate Rac targeting by internalization of membrane domains. *Science* **303**, 839-842.
DerMardirossian, C. and Bokoch, G. M. (2005). GDIs: central regulatory molecules in Rho GTPase activation. *Trends Cell Biol.* **15**, 356-363.
Dovas, A. and Couchman, J. R. (2005). RhoGDI: multiple functions in the regulation of Rho family GTPase activities. *Biochem. J.* **390**, 1-9.
Gandhi, P. N., Gibson, R. M., Tong, X., Miyoshi, J., Takai, Y., Konieczkowski, M., Sedor, J. R. and Wilson-Delfosse, A. L. (2004). An activating mutant of

Rac1 that fails to interact with Rho GDP-dissociation inhibitor stimulates membrane ruffling in mammalian cells. *Biochem. J.* **378**, 409-419.

García-Mata, R., Wennerberg, K., Arthur, W. T., Noren, N. K., Ellerbroek, S. M. and Burridge, K. (2006). Analysis of activated GAPs and GEFs in cell lysates. *Methods Enzymol.* **406**, 425-437.

Grashoff, C., Hoffman, B. D., Brenner, M. D., Zhou, R., Parsons, M., Yang, M. T., McLean, M. A., Sligar, S. G., Chen, C. S., Ha, T. et al. (2010). Measuring mechanical tension across vinculin reveals regulation of focal adhesion dynamics. *Nature* **466**, 263-266.

Jaffe, A. B. and Hall, A. (2005). Rho GTPases: biochemistry and biology. *Annu. Rev. Cell Dev. Biol.* **21**, 247-269.

Kiessling, V., Crane, J. M. and Tamm, L. K. (2006). Transbilayer effects of raft-like lipid domains in asymmetric planar bilayers measured by single molecule tracking. *Biophys. J.* **91**, 3313-3326.

Meerbrey, K. L., Hu, G., Kessler, J. D., Roarty, K., Li, M. Z., Fang, J. E., Herschkowitz, J. I., Burrows, A. E., Ciccia, A., Sun, T. et al. (2011). The pINDUCER lentiviral toolkit for inducible RNA interference in vitro and in vivo. *Proc. Natl. Acad. Sci. USA* **108**, 3665-3670.

Melkonian, K. A., Ostermeyer, A. G., Chen, J. Z., Roth, M. G. and Brown, D. A. (1999). Role of lipid modifications in targeting proteins to detergent-resistant membrane rafts. Many raft proteins are acylated, while few are prenylated. *J. Biol. Chem.* **274**, 3910-3917.

Michaely, P. A., Mineo, C., Ying, Y. S. and Anderson, R. G. (1999). Polarized distribution of endogenous Rac1 and RhoA at the cell surface. *J. Biol. Chem.* **274**, 21430-21436.

Moissoglu, K., Slepchenko, B. M., Meller, N., Horwitz, A. F. and Schwartz, M. A. (2006). In vivo dynamics of Rac-membrane interactions. *Mol. Biol. Cell* **17**, 2770-2779.

Moissoglu, K., McRoberts, K. S., Meier, J. A., Theodorescu, D. and Schwartz, M. A. (2009). Rho GDP dissociation inhibitor 2 suppresses metastasis via unconventional regulation of RhoGTPases. *Cancer Res.* **69**, 2838-2844.

Navarro-Lérida, I., Sánchez-Perales, S., Calvo, M., Rentero, C., Zheng, Y., Enrich, C. and Del Pozo, M. A. (2012). A palmitoylation switch mechanism regulates Rac1 function and membrane organization. *EMBO J.* **31**, 534-551.

Prior, I. A., Harding, A., Yan, J., Sluimer, J., Parton, R. G. and Hancock, J. F. (2001). GTP-dependent segregation of H-ras from lipid rafts is required for biological activity. *Nat. Cell Biol.* **3**, 368-375.

Roberts, P. J., Mitin, N., Keller, P. J., Chenette, E. J., Madigan, J. P., Currin, R. O., Cox, A. D., Wilson, O., Kirschmeier, P. and Der, C. J. (2008). Rho Family GTPase modification and dependence on CAAX motif-signaled posttranslational modification. *J. Biol. Chem.* **283**, 25150-25163.

Schmidt, M., Schmidt, M. F. and Rott, R. (1988). Chemical identification of cysteine as palmitoylation site in a transmembrane protein (Semliki Forest virus E1). *J. Biol. Chem.* **263**, 18635-18639.

Stites, E. C., Trampont, P. C., Ma, Z. and Ravichandran, K. S. (2007). Network analysis of oncogenic Ras activation in cancer. *Science* **318**, 463-467.

van Rheenen, J., Song, X., van Roosmalen, W., Cammer, M., Chen, X., Desmarais, V., Yip, S. C., Backer, J. M., Eddy, R. J. and Condeelis, J. S. (2007). EGF-induced PIP2 hydrolysis releases and activates cofilin locally in carcinoma cells. *J. Cell Biol.* **179**, 1247-1259.

Wan, C., Kiessling, V., Cafiso, D. S. and Tamm, L. K. (2011). Partitioning of synaptotagmin I C2 domains between liquid-ordered and liquid-disordered inner leaflet lipid phases. *Biochemistry* **50**, 2478-2485.

Yoshizaki, H., Ohba, Y., Kurokawa, K., Itoh, R. E., Nakamura, T., Mochizuki, N., Nagashima, K. and Matsuda, M. (2003). Activity of Rho-family GTPases during cell division as visualized with FRET-based probes. *J. Cell Biol.* **162**, 223-232.